NOTES AND CORRESPONDENCE

Nonlinear Effects in Coupled Atmosphere–Ocean Basin Modes*

Y. WAKATA** AND E. S. SARACHIK***

**School of Marine Science and Technology, Tokai University, Shimizu, Shizuoka, Japan
***Department of Atmospheric Sciences, University of Washington, Seattle, Washington

7 April 1993 and 16 August 1993

ABSTRACT

The effect of nonlinearities on a previously investigated coupled atmosphere–ocean basin mode is examined. The nonlinearity in the thermodynamic equation for sea surface temperature arises mainly from the dependence of subsurface temperature on the thermocline depth anomaly in the parameterization of entrainment into the mixed layer. This nonlinearity ultimately suppresses the linear growth of the unstable mode and equilibrates it at a finite amplitude. Because this nonlinearity acts differently for warm and cold states, the warm states are enhanced at finite amplitude. It is found that multiple equilibrium states appear as the coupling coefficient increases and as the reflection coefficient of the oceanic Rossby mode at the western boundary decreases. The finite-amplitude warm equilibrium state turns out to be stable, but the finite-amplitude cold state is unstable. The explicit inclusion of the dependence of the coupling strength on the warm and cold sea surface temperature anomalies modulates the sinusoidal-like oscillation and increases the period, but aperiodic solutions could not be obtained.

1. Introduction

The stability of coupled atmosphere–ocean modes in and over a bounded ocean basin was investigated by Wakata and Sarachik (1991b, hereafter referred to WS) using a linear eigenvalue technique to explain the El Niño–Southern Oscillation (ENSO) phenomenon found in the Cane–Zebiak (Zebiak and Cane 1987) model. In this note, the effects of nonlinearities on this linear coupled basin mode will be investigated.

In the WS calculations, the ocean is bounded by rigid walls at its eastern and western edges and the atmosphere is assumed to be cyclic around the earth. The atmosphere and the ocean interact as follows. The atmosphere is heated in proportion to the sea surface temperature anomaly (SSTA) provided by the ocean, and the ocean is driven by stress in proportion to the surface wind velocity provided by the atmosphere. Assuming realistic profiles of the basic-state quantities, especially the narrow meridional extent of the oceanic upwelling near the equator, WS obtained an unstable mode that exhibits many of characteristics of ENSO, a long period oscillation of the SSTA in the eastern Pacific that displays nonpropagating onsets. Wakata and Sarachik noted that if the meridional extent of the upwelling is wide, the unstable mode propagates eastward, but if it is narrow, the mode ceases to propagate and instead grows in place as in the Cane–Zebiak model.

In the linear problem, some questions still remain. How does the exponential growth of the linear unstable basin mode eventually get suppressed by the nonlinearities? Can nonlinearities change the essential results of the linear theory, say by so distorting the periodic oscillations that they are no longer recognizable, or by inducing nonperiodic oscillations?

The purpose of this note is to address these questions. The linear model in WS was reformulated to include a number of specific nonlinearities. Since the model in WS was obtained by linearizing the model of Zebiak and Cane (1987, referred to as ZC), the nonlinear terms are obtained from their model. In particular, the nonlinear entrainment term and the east–west advection term are included in the oceanic thermodynamic equation. Another nonlinear effect is the coupling strength between the ocean and atmosphere as a function of anomalous SST.

In order to motivate the paper, we examine the difference between the linear and nonlinear retarded oscillator equation. As Battisti and Hirst (1989) showed, the oscillatory properties of the SST anomalies in the ZC model can be obtained as an analog to the linearized ZC model:

* JISAO Contribution Number 221.

Corresponding author address: E. S. Sarachik, Dept. of Atmospheric Sciences, AK-40, University of Washington, Seattle, WA 98195.

$$\frac{dT(t)}{dt} = cT(t) - bT(t-\tau). \quad (1)$$

This equation has growing unstable oscillatory solutions only when $b > c$, where c is mainly a function of the local coupling and b gives the amplitude of the retarded response.

In the presence of nonlinearities, the simplest nonlinear analog of the retarded oscillator equation becomes (Suarez and Shopf 1988)

$$\frac{dT(t)}{dt} = cT(t) - bT(t-\tau) - gT^3(t), \quad (2)$$

which has the same oscillatory properties as the linear retarded oscillator equation (when $b > c \gg g$) except that the amplitude is now equilibrated by the nonlinear terms. This is known from the work of Battisti and Hirst (1989), who pointed out that the prime nonlinearity arises from the dependence of the subsurface temperature on thermocline depth [see Eq. (5) below].

Suarez and Schopf (1988) argued that when $c > b$, there are *steady* finite amplitude solutions to (2) and the oscillations are intrinsically nonlinear. The steady finite-amplitude solutions are

$$T = \pm\left[\frac{c-b}{g}\right]^{1/2}, \quad (3)$$

and Schopf and Suarez argued that an intrinsically nonlinear oscillation exists, oscillating between these two finite-amplitude states. On the basis of this simple argument, we would expect that as the local coupling increases and the retarded response decreases (i.e., as c grows and b decreases so that c eventually exceeds b) multiple finite-amplitude equilibrium states arise. We will take these simple arguments as guidance and seek multiple equilibria in the nonlinear coupled model as a function of increased air–sea coupling and decreased ocean reflection coefficient at the western boundary.

We might note that Anderson and McCreary (1985) and Battisti and Hirst (1989) found a warm equilibrium state in their air–sea coupled models, but cold equilibria have not been found by time-dependent models. An iterative procedure will permit us to obtain cold equilibrium states in the nonlinear atmosphere–ocean coupled model, but they turn out to be unstable, explaining why they could not be found by time-marching methods.

In this research, variables in the east–west direction are discretized on a grid while variables in the north–south direction are expanded in series of Hermite functions. The simultaneous equations for the time evolution of the variables on the grids are obtained, and are solved either by time integration or iterative methods.

2. The model

The governing equations are the same as those of WS except that, instead of the linearized thermodynamic equation, we keep the full nonlinear thermodynamic equation used by ZC. The reduced gravity linearized shallow-water equations in the long-wave approximation are used for the dynamics in both the ocean and atmosphere. The atmosphere is assumed to be in steady state with the underlying SST, since the atmospheric adjustment time is fast compared with the time scale of the ocean and with the time scale of the ENSO cycle.

For analytical tractability, the atmospheric model does not include the convergence feedback included in ZC; hence, the geopotential of the atmosphere is changed only by the latent heating in proportion to the anomaly of sea surface temperature, with proportionality constant K_Q. The ocean is driven by a wind stress field, parameterized as a linear function of the winds with proportionality constant K_S. These are the same assumptions used in WS.

The dynamical governing equations are the same as those of Hirst [1988, Eq. (10)] and we follow his notation hereafter. However, as in WS, we use the value of parameters adopted by ZC, shown in Table 1.

The thermodynamic equation for the SST anomalies adopted by ZC is simplified as

$$\frac{\partial T}{\partial t} = -u(\bar{T}_x + T_x) - nT - \gamma\frac{\bar{w}_s}{H_1}(T - T_s), \quad (4)$$

where the first term in the right-hand side is horizontal advection with $\bar{T}_x = -5.0 \times 10^{-7} \exp[-(7-i)^2/4^2] \times \exp(-y^2/2)$ K m^{-1}, where i is a grid number in the latitudinal direction (shown in Fig. 3) and y is a meridional coordinate scaled by the equatorial radius of deformation, the second term is Newtonian damping with $n = (125 \text{ days})^{-1}$, and the last term is the cooling

TABLE 1. Values for the basic parameters. Symbols follow the convention of Hirst (1988).

Atmospheric Rayleigh friction coefficient (A)	(2 days)$^{-1}$
Atmospheric Newtonian cooling coefficient (B)	(2 days)$^{-1}$
Oceanic Rayleigh friction coefficient (a)	(2.5 years)$^{-1}$
Damping coefficient for h field (b)	(2.6 years)$^{-1}$
Oceanic Newtonian cooling coefficient (d)	(26 days)$^{-1}$ on the equator (125 days)$^{-1}$ in high latitude
Oceanic gravity wave speed (C_o)	2.9 m s^{-1}
Atmospheric gravity wave speed (C_a)	60.0 m s^{-1}
Wind stress heating coupling coefficient (K_S)	1.7×10^{-7} s^{-1}
Atmospheric heating coupling coefficient (K_Q)	5.1×10^{-3} m^2 s^{-3} K^{-1}
Background zonal SST gradient in the central Pacific (T_x)	-5.0×10^{-7} K m^{-1}
Vertical advection thermal forcing coefficient (K_T)	7.95×10^{-8} K m^{-1} s^{-1}

effect due to the entrainment of colder water into the mixed surface layer. The subsurface temperature T_s is nonlinearly parameterized in terms of the thermocline depth in the same way as ZC as

$$T_s = A[\tanh(B(\bar{h} + |h|)) - \tanh(B\bar{h})], \quad (5)$$

where $A = 28$ K and $B^{-1} = 80$ m for $h > 0$, and $A = -40$ K and $B^{-1} = 33$ m for $h \leq 0$. Here $\bar{h} = \bar{h}(x)$ is the thermocline depth of the basic state on the equator, taken to be

$$\bar{h} = -P \tanh \frac{x - x_c}{R} + Q \quad (6)$$

where the typical values are $P = 50$ m, $Q = 100$ m, $x_c = 9\delta x = 10\,350$ km, and $R = 2\delta x = 2302$ km ($\delta x = 1151$ km is the grid interval). The thermocline depth is then 150 m in the western end of the Pacific and 50 m in the east. Note that in Eq. (5) the nonlinearity is of two forms: one in that the shape of the T_s is of intrinsically nonlinear form, the other in that there is a discontinuity at zero height anomaly.

The entrainment velocity is assumed to have the form

$$w_s = \langle w_s \rangle \exp(-\alpha y^2), \quad (7)$$

where $\langle w_s \rangle$ is an entrainment velocity on the equator and $\alpha^{-1/2}$ is a meridional e-folding length. From Ekman boundary-layer theory, the typical values are evaluated as $\langle w_s \rangle = 2$ m day^{-1} and $\alpha^{-1/2} = 146$ km as discussed in WS.

3. Results

A simultaneous set of 217 nonlinear equations is obtained by expanding the equations in an even Hermite function series up to the 14th mode in the latitudinal direction (assuming latitudinal symmetry about the equator), and divided into 15 grid points in the longitudinal direction as in Hirst (1988). These equations were solved by a time integration method for investigating the time-dependent behavior and, after zeroing the time derivative terms, by an iterative method based on Newton's method (using a subroutine in MATLAB) for investigating the steady equilibrium solutions.

a. Presence of equilibrium states

A map showing the area where equilibrium states appear is depicted in the parameter space of the coupling coefficient K_Q and the reflection coefficient δ of the Rossby mode at the western boundary in Fig. 1. The zero amplitude equilibrium solutions, whose variables (i.e., u, v, h, T, etc.) are all zero, exist at all points of this space: the stability analysis about this zero state corresponds to the linear stability problem discussed by WS. The dotted line in Fig. 1 corresponds to the neutral stability line for this zero state: points to the left of this line correspond to weaker coupling and are linearly stable, and points to the right are unstable.

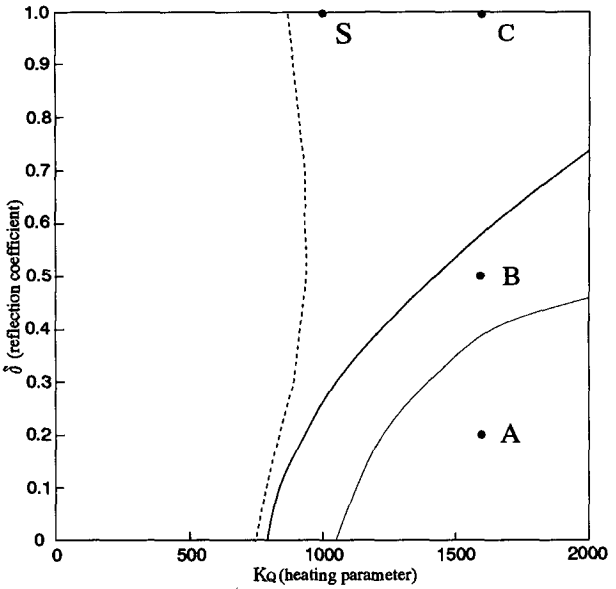

FIG. 1. Diagram for equilibrium states in the space of the coupling constant vs Rossby reflection coefficient. The dashed line is the neutral line of the linear stability problem about the zero amplitude state: the zero state is linearly stable to the left of this line and unstable to the right. To the right of the thick solid line, warm finite-amplitude equilibrium states can exist. To the right of the thin solid line, cold and warm states can exist. The points A, B, C, and S are described in the text.

Wakata and Sarachik adopted standard values of the heating coefficient $K_Q = 1000$ and the reflection coefficient $\delta = 1$, both estimated using the ZC model. In this note, these same external parameters, indicated by the point S in Fig. 1, are also taken as standard parameters. At this standard point, the solution with all physical (anomaly) quantities equal to zero is weakly unstable.

Nontrivial finite-amplitude equilibrium solutions also exist in parts of the parameter space. The difference of the coefficient in the thermodynamic Eq. (5) for positive and negative depth anomalies makes the linear eigenvalue problem about the zero amplitude state ambiguous: in WS the averaged coefficient for the positive and negative cases is used. In this nonlinear case, the stability is evaluated by calculating the growth or decay of a small anomaly (whether positive or negative) added to the equilibrium state by solving the time evolution equations using the actual values of Eq. (5). The investigation of the stability for the nontrivial equilibrium states is done by this method.

Warm finite-amplitude equilibrium states appear with increasing coupling coefficient K_Q and decreasing reflection coefficient δ of the Rossby mode at the western boundary. Cold finite-amplitude equilibrium states appear at still larger coupling coefficient and still lower values

of the reflection coefficient and exist to the right of the thick solid line in Fig. 1. To the right of the thin solid line, warm and cold finite-amplitude equilibria can coexist.

The eastern Pacific SSTA (at longitude 12 in Fig. 3) for the finite-amplitude equilibrium states is plotted against the coupling coefficient in Fig. 2, with the contours labeled by the Rossby reflection coefficient δ. As the coupling coefficient increases, a pair of positive and negative equilibrium solutions appears, as in a pitchfork-type bifurcation. The bifurcation points from the zero solution to the positive: the negative solutions do not coincide since the entrainment temperatures T_s for the mixed-layer depth anomaly $h \to 0-$ and $h \to 0+$ are not continuous. Since the discontinuity of this sort is not present in nature and comes from the mathematical simplification in Eq. (5) the appearance of the multiple equilibrium solutions is in substance a pitchfork type.

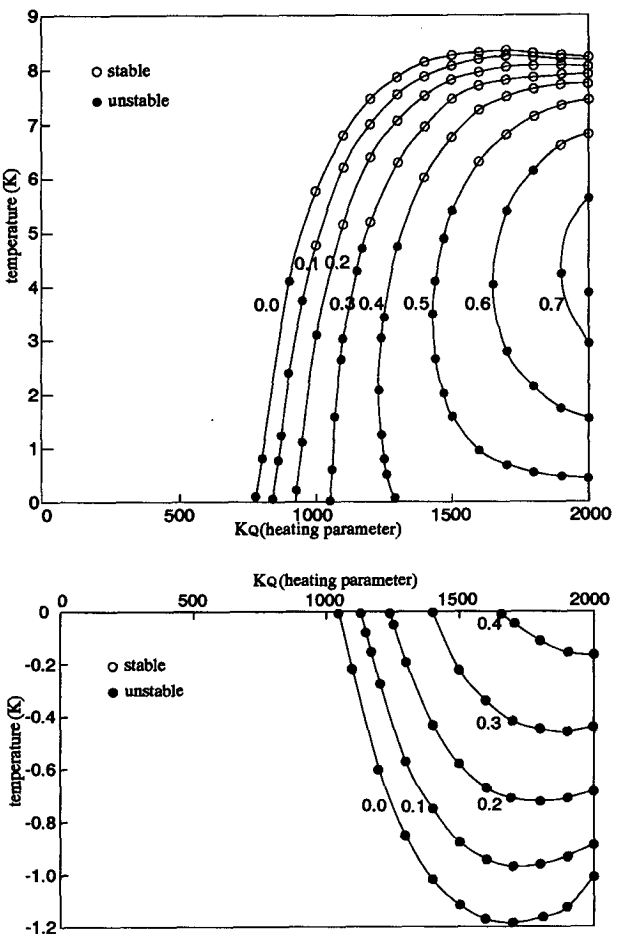

FIG. 2. Sea surface temperature in the eastern Pacific vs the coupling parameter: the lines are labeled by the value of the reflection coefficient for the Rossby mode at the western boundary. (a) Warm equilibria and (b) cold equilibria. Symbol (○) indicates stable equilibrium states and (●) unstable.

The warm finite-amplitude equilibrium states show a supercritical-type bifurcation in Fig. 2a, which has two solutions appearing for each value of the coupling constant for large enough values of the reflection coefficient. The large amplitude states are stable but become unstable near the bending-type bifurcation point. The small amplitude warm states are always unstable.

The cold (negative SSTA) finite-amplitude equilibrium states are shown in Fig. 2b. *Every cold equilibrium solution is unstable.* The absolute value of SSTA in the cold equilibrium states is smaller than those of the warm states.

b. *Structure of equilibrium states*

The structure of the equilibrium solutions is discussed in this paragraph. For large enough coupling parameter and small enough reflection coefficient, warm and cold equilibrium states can coexist at the same parameters. The structure of the two states at point A in Fig. 1 ($K_Q = 1600$, $\delta = 0.2$) is shown in Figs. 3a and 3b, respectively. For the warm state, the mixed-layer depth anomaly is shallow in the western basin and deep in the eastern basin. The response of the low-order Rossby mode can be clearly seen in the western basin. By contrast, the Kelvin-type response is not clear in the eastern basin. The reflection at the eastern boundary can be seen off the equator: these modes correspond to the higher Rossby modes. In the eastern basin, the SSTA is high and positive, somewhere near 10 K. This unrealistically high value comes from the assumption of a stronger than standard coupling constant. Westerly surface winds blow in the central basin and the pressure decreases in the eastern basin: these characteristics are similar to the warm phase of ENSO.

The cold equilibrium state for these external parameters is shown in Fig. 3b. The eastern basin is cold and has a shallow thermocline, while the thermocline in the western basin is deep. The long Rossby mode response with negative depth anomaly is seen in the off-equatorial area. Easterly surface wind anomalies blow in the equatorial region.

Figure 4 shows the two warm multiple equilibrium states for $K_Q = 1600$ and reflection coefficient $\delta = 0.5$, indicated by point B in Fig. 1. The stable warm state in Fig. 4a is similar to that of Fig. 3a. The small amplitude warm state shown in Fig. 4b has a relatively large amplitude of the depth anomaly in the western basin. The SSTA peaks slightly in the central ocean around $y = 1$ in the meridional coordinate. This comes from the effect of nonlinear advection in the thermodynamic equation. Calculations without this advection term do not show the supercritical-type bifurcation, so they do not show this small amplitude warm equilibrium.

c. *Time evolution*

As discussed in the previous section, there are some regions of parameter space that have finite-amplitude

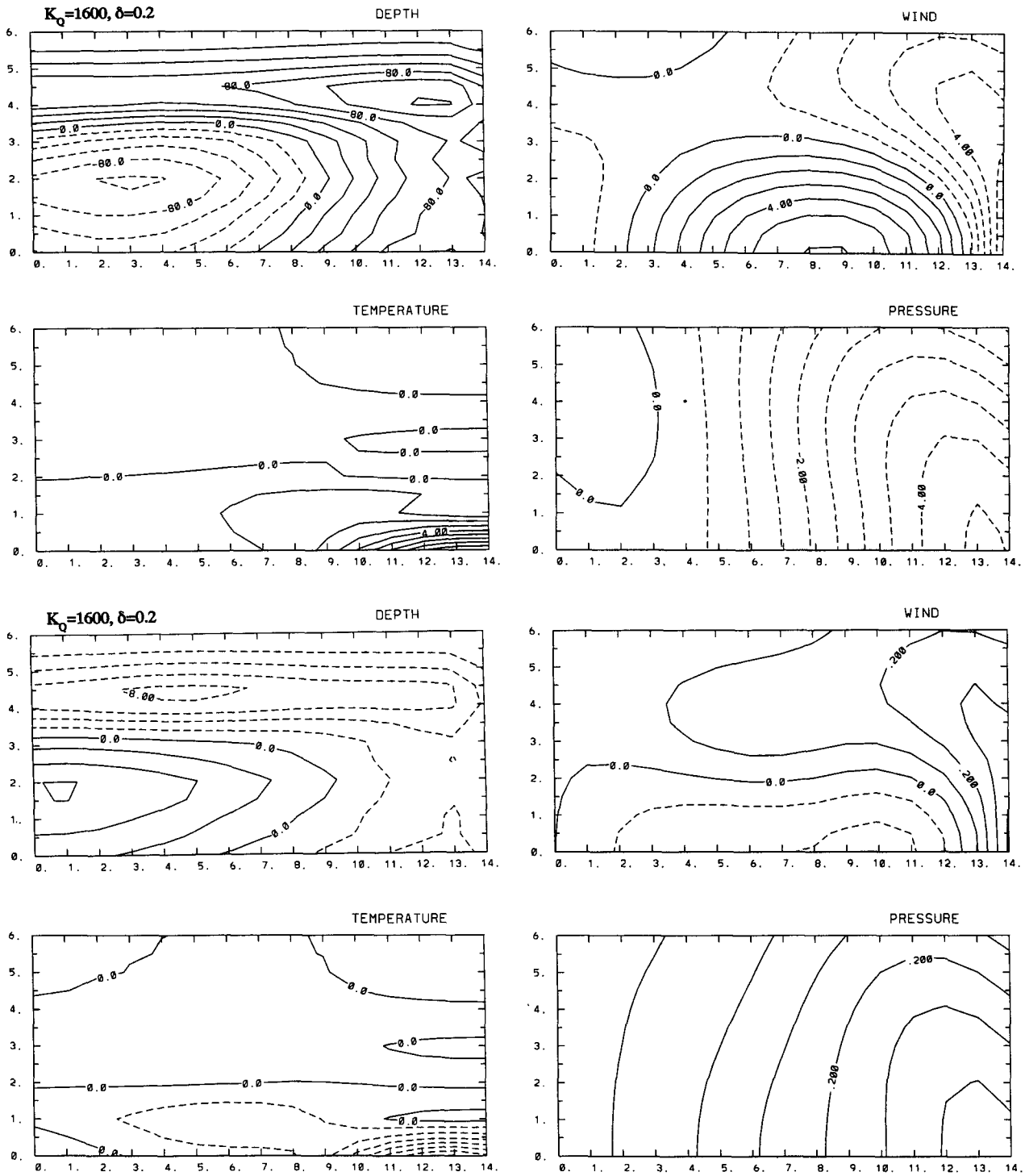

FIG. 3. (a) Stable warm equilibrium state with coupling parameter $K_Q = 1600$ and reflection coefficient $\delta = 0.2$ (indicated by point A in Fig. 1). The contour intervals are 20 m (depth anomaly), 1 K (SSTA), 1 m s^{-1} (wind), and 0.5 mb (atmospheric pressure). (b) Cold equilibrium state (contour intervals are 2 m, 0.1 K, 1 m s^{-1}, and 0.5 mb, respectively). The abscissa is longitude in units of grid size (1151 km). The ordinate is latitude in units of equatorial Rossby deformation length (356 km) with zero at the equator.

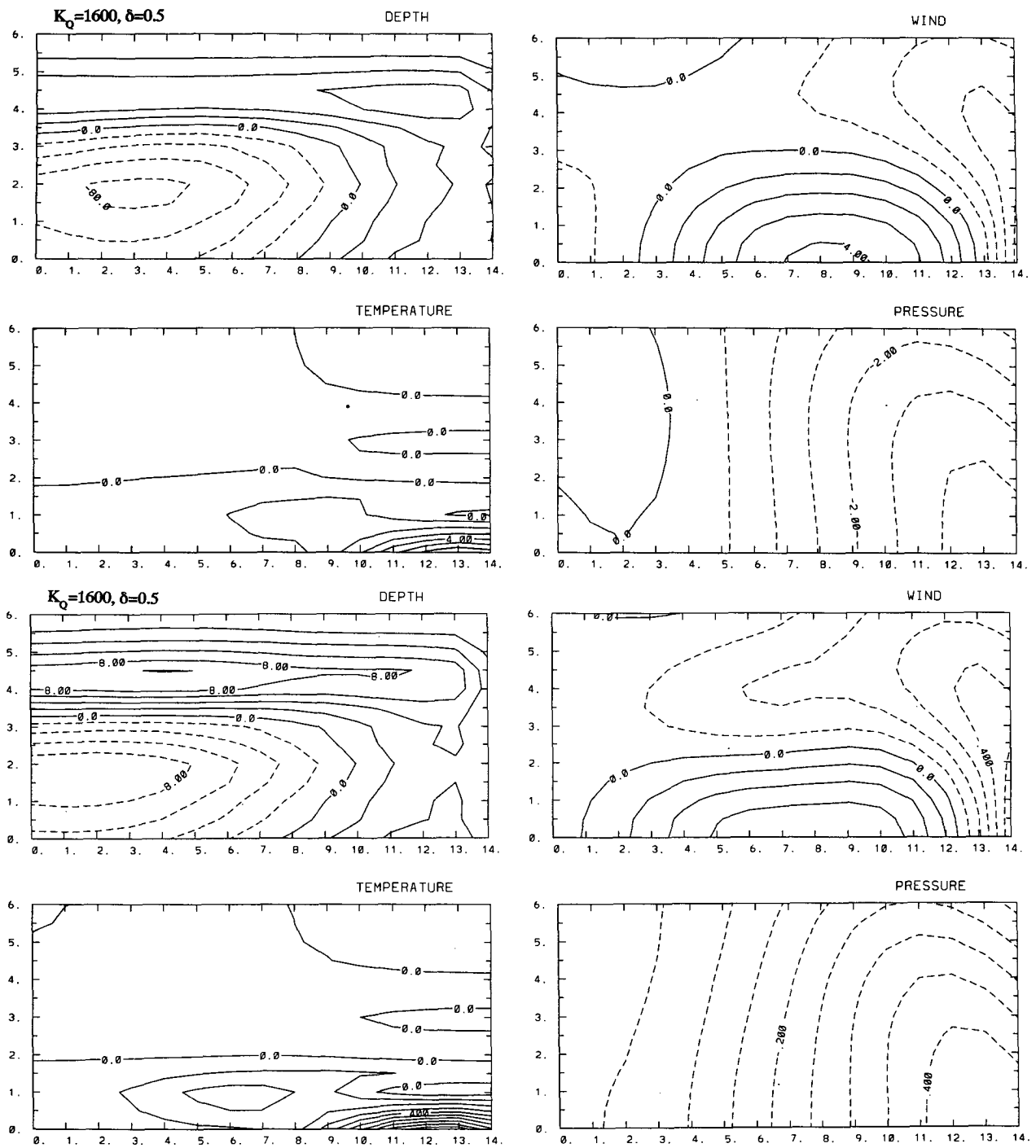

FIG. 4. (a) Large amplitude warm equilibrium state for $K_Q = 1600$, $\delta = 0.5$ indicated by B in Fig. 1 (contour intervals are 20 m, 1 K, 1 m s^{-1}, and 0.5 mb, respectively). (b) Small amplitude warm equilibrium state (contour intervals are 2 m, 0.1 K, 0.1 m s^{-1}, and 0.05 mb).

multiple equilibrium solutions. Here we are interested in how these equilibrium states evolve in time and whether or not periodic or nonperiodic solutions appear. For this purpose, we must solve the time evolution equations.

The first case examined is the standard case solution with the parameters used by ZC (point S in Fig. 1). The reflection coefficient at the western boundary is $\delta = 1$ so that the Rossby mode reflects perfectly, and the

coupling coefficient is $K_Q = 1000$. This point has only a zero equilibrium state and is slightly unstable away from the zero state. As shown by WS, the state is oscillatory and grows exponentially in time when nonlinearities are absent.

Figure 5 shows the time evolution of SSTA on the equator at longitude 12 in Fig. 3 in the eastern Pacific for the various cases. Figure 5a shows the time series for a perturbation about the standard zero state where the initial condition was chosen to have slightly warm SSTA as in the eastern Pacific with all the other variables set to zero. The state grows and eventually oscillates with finite amplitude, having maximum value 2.5 K and minimum −1.5 K. This asymmetry is due to the previously mentioned asymmetry of the thermodynamic equation emphasizing the warm phase over the cold phase in this oscillation. The period is about 2.5 years. Figure 6 shows the time series for one period, which is very close to the linear result of WS. We see that the results from the linear stability problem are applicable to the case for the standard external parameters, with the major effects of nonlinearities being to equilibrate the oscillation at finite amplitude and to induce the asymmetry of the warm and cold phases. This is similar to the conclusion of Battisti and Hirst (1989).

The second case examines the case with $\delta = 0.5$ and $K_Q = 1600$, indicated by point B in Fig. 1, where there are multiple equilibrium solutions: a large and small warm solution and the zero solution. The time-dependent behavior is shown in Fig. 5b. The initial condition was selected to be at the large finite-amplitude warm equilibrium state, which has an SSTA of 6.29 K at the longitude 12 on the equator. Since this state is locally stable, the SSTA stays constant. If instead the initial condition were selected to be the small finite-amplitude warm state (which is marginally unstable according to Fig. 2a), the SSTA grows and subsequently oscillates with period 1200 days. This is a true nonlinear oscillation and the closest we could come to the nonlinear Schopf–Suarez oscillation mentioned with regard to Eq. (2). It should also be clear that nonlinearities in the atmosphere–ocean coupled system induce a dependence on the initial conditions due to the existence of multiple equilibria. The region of parameter space that shows this dependence on initial conditions could not be clearly defined.

Further decreasing the reflection coefficient to $\delta = 0.2$ (point A in Fig. 1) now gives warm and cold finite-amplitude equilibrium states. The initial condition was set to be the cold equilibrium state. This cold equilibrium is unstable according to linear theory, but if the initial perturbation away from the equilibrium solution is kept extremely small, a long time is needed for the unstable mode to grow. The SSTA stays constant up to 2200 days and then jumps from the cold equilibrium to the warm equilibrium at a time near 2400 days (Fig. 5d). In this range of small reflection coefficients, oscillatory solutions about the finite-amplitude equilibria could not found.

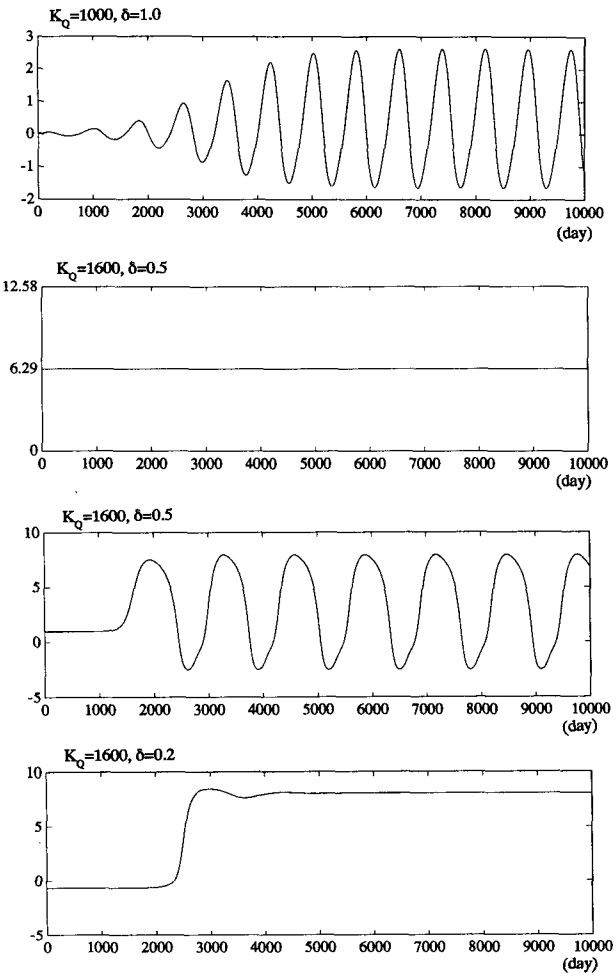

FIG. 5. Time evolution of SSTA in the eastern Pacific. (a) Standard case. $K_Q = 1000$, $\delta = 1$ (point S in Fig. 1). (b) Initial condition is large amplitude positive stable equilibrium state in Fig. 4a for $K_Q = 1600$, $\delta = 0.5$ (point B in Fig. 1). (c) Initial condition is small amplitude unstable equilibrium state in Fig. 4b for $K_Q = 1600$, $\delta = 0.5$ (point B in Fig. 1). (d) Initial condition is small amplitude cold equilibrium state in Fig. 3b for $K_Q = 1600$, $\delta = 0.2$ (point A in Fig. 1).

Figure 7 shows how the cold state of Fig. 5d dissolves and the warm state is realized. The structure at 2200 days is hardly different from the cold equilibrium state shown in Fig. 3b. The eastern basin is cold, positive depth anomalies are present near the equatorial area in the western basin, and negative anomalies are present in the off-equatorial region. This solution changed rapidly at 2400 days. The propagating Kelvin mode can be seen in the eastern basin as the surface is warmed. At day 2600, the higher Rossby mode near $y = 4$ in the western Pacific disappears and the structure approaches that in the growth stage of the positive

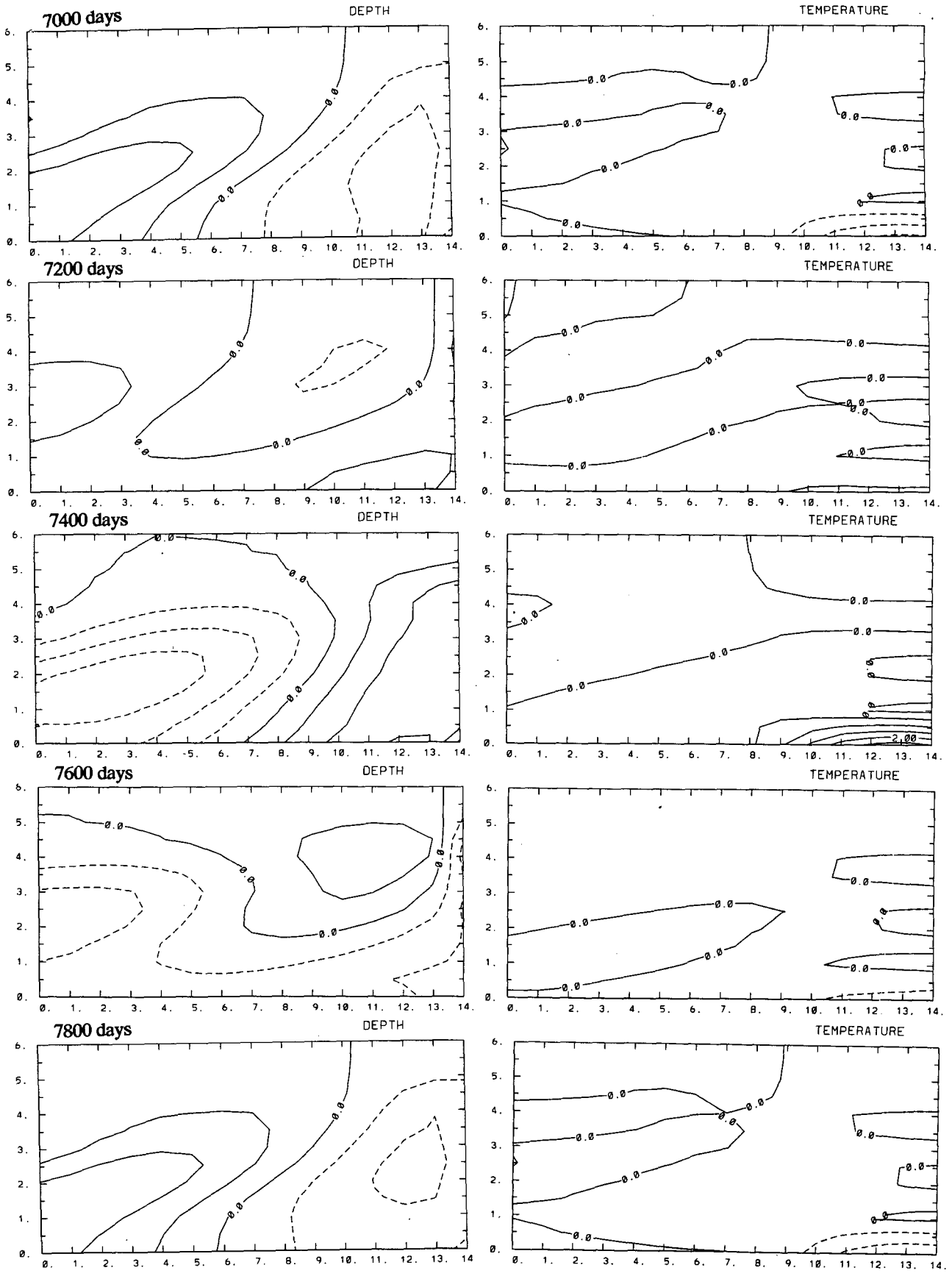

anomaly of the linear unstable basin mode discussed by WS. After 2800 days, gradually the positive off-equatorial Rossby mode expands westward. The depth in the eastern Pacific is not changed, because the negative Kelvin mode, produced through the reflection of the negative Rossby mode seen in the western Pacific, is small owing to the small reflection coefficient. The time-dependent solution approaches the warm equilibrium state at 4000 days and the warm equilibrium solution subsequently appears.

d. Nonlinear effects in the atmosphere

Atmospheric heating also has nonlinear processes associated with it. In the ZC model, the anomalous heating of the atmosphere is related to the anomalous convergence of the moisture in the lower atmosphere as well as to the SSTA. This occurs because the precipitation is the local evaporation plus the moisture convergence—the precipitation clearly must be positive. The anomalous precipitation is the total precipitation less the climatological precipitation (the latter two constrained to be positive) and, if the total convergence is less than the climatological convergence, the anomalous precipitation will be negative.

It is difficult to include this process into our simple model. But if the ocean is very cold, the atmospheric pressure becomes high and the low-level wind field could become divergent and the interaction of the atmosphere and ocean may weaken. We include this effect as follows.

We will assume that the strength of the anomalous heating of the atmosphere is proportional to the SSTA unless the SST anomaly falls below a critical value ΔT_c, in which case the atmospheric heating is assumed to be a constant:

$$Q = \begin{cases} K_Q T & \text{if} \quad T > \Delta T_c \\ K_Q T_c & \text{if} \quad T < \Delta T_c. \end{cases} \tag{8}$$

We choose $\Delta T_c = -0.5$ K. We thus assume that the atmosphere–ocean coupling becomes weaker in the cold phase than the warm phase. The result for the external parameters $K_Q = 1600$, $\delta = 1$ (point C in Fig. 1) is shown in Fig. 8. The transition from the cold state to the warm state does not occur immediately: the cold state maintains itself and then rapidly changes to the warm state. This happens because the positive Rossby mode weakens (owing to the weaker atmosphere–ocean coupling) so that the reflected Kelvin mode also weakens, thereby slowing the transition from the cold state to the warm. The sinusoidal-like oscillation without the nonlinearities of Eq. (8) (depicted by the solid line in Fig. 8) is modulated by the inclusion of these nonlinearities (the dotted line in Fig. 8), but nonperiodic behavior is not obtained.

4. Conclusions and discussion

The effects of nonlinearities on atmosphere–ocean coupled basin modes have been investigated in this note. For the standard parameters of the ZC model, it was found that the nonlinear effects associated with entrainment in the thermodynamic equation can suppress the exponential growth estimated from the linear theory and equilibrate the coupled mode at finite amplitude. The period of the oscillation is close to that estimated from the linear theory. This shows that the major results of the linear theory are applicable to the standard parameter range of the ZC model, as was previously indicated by Battisti and Hirst (1989).

The effect of nonlinearities was investigated for an unusually wide range of the external parameters for the following reasons. First, to understand the behavior of the nonlinear system for specific external parameters, we should be able to identify these behaviors under changes of the external parameters. Second, the standard parameters used in ZC are not unambiguously known and may have some uncertainty arising from the simplifications of the basic equations.

The equilibrium solutions of this coupled atmosphere–ocean system were investigated. For the standard external parameters ($K_Q = 1000$, $\delta = 1$) the only equilibrium solution was the zero solution. As the Rossby reflection coefficient is reduced and the coupling parameter is increased, finite-amplitude warm equilibria appear and subsequently finite-amplitude cold equilibria appear.

The amplitudes of the warm equilibria are larger than those of the cold equilibria due to the difference of the strength of the atmosphere–ocean coupling. Their stability properties are also different. The warm state is stable except in the region of the bifurcation point, but the cold state is unstable everywhere. This may explain why Anderson and McCreary (1985) and Battisti and Hirst (1989) can find warm equilibria but not cold in their time evolution models.

The delayed oscillator equation discussed by Suarez and Schopf (1988) and Battisti and Hirst (1989) to explain the slow oscillation of the warm and cold states shows the appearance of the two equilibrium states, but in their cases these have the same amplitude but opposite signs. The stability of the two states is also similar and is stable for strong coupling, as discussed by

FIG. 6. Time evolution of the thermocline depth anomaly and SSTA for the case in Fig. 5a. The contour intervals are 5 m (for thermocline depth) and 0.5 K (for SSTA).

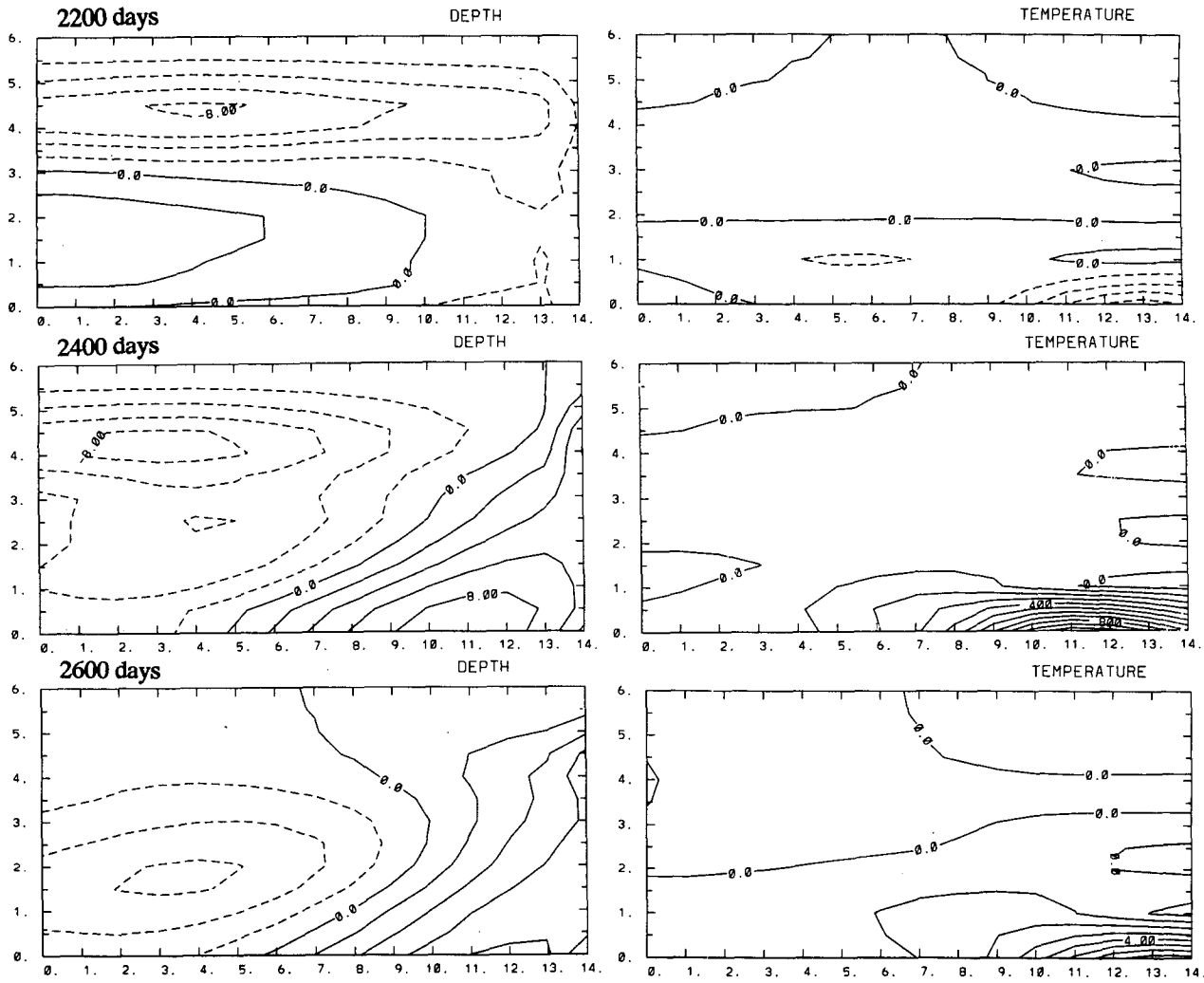

FIG. 7. As in Fig. 6 but for the case of Fig. 5d (2200 ~ 4000 days). The contour intervals are 2 m (depth anomaly) and 0.1 K (SSTA), and change to 20 m and 1 K for 2800 ~ 4000 days.

Battisti and Hirst (1989). This symmetry of the equilibrium states for both signs of the anomalies can be easily explained. The delayed oscillator equation originally has a symmetry about the sign of the temperature: this equation is unchanged by the transformation from T to $-T$. In the presence of a T^3 nonlinearity, this symmetry is maintained.

Our results differ from theirs because the fundamental nonlinearity comes from the nonlinear feedback in the temperature of the entrained water. If the mixed layer deepens, the temperature of the entrained water warms in proportion to the depth anomaly for small anomalies but saturates at a finite value for large anomalies thereby giving a negative feedback. Expanding the form in Eq. (5) in a Taylor series yields a T^2 term, and including this term in the delayed oscillator equation breaks the symmetry of the equation and induces different stability properties for positive and negative signs of the SSTAs. Horizontal advection of temperature will also contribute to breaking the symmetry.

The nonlinearity of the atmosphere, which weakens the atmosphere–ocean coupling for cold SSTAs, sinusoidally modulates the periodic oscillation and lengthens the period. However, this nonlinearity did not induce nonperiodic behavior. To induce nonperiodicity in these equations, we would probably need to include random forcing in the atmosphere. We speculate that the cold state, in which the coupling is weak and the memory of oscillation is presumably also weak, would be more easily affected by the external forcing, but this remains a topic for further research.

The fundamental oscillation mechanism is the delayed oscillator mechanism. However, to consistently include the nonlinearities, the retarded oscillator should

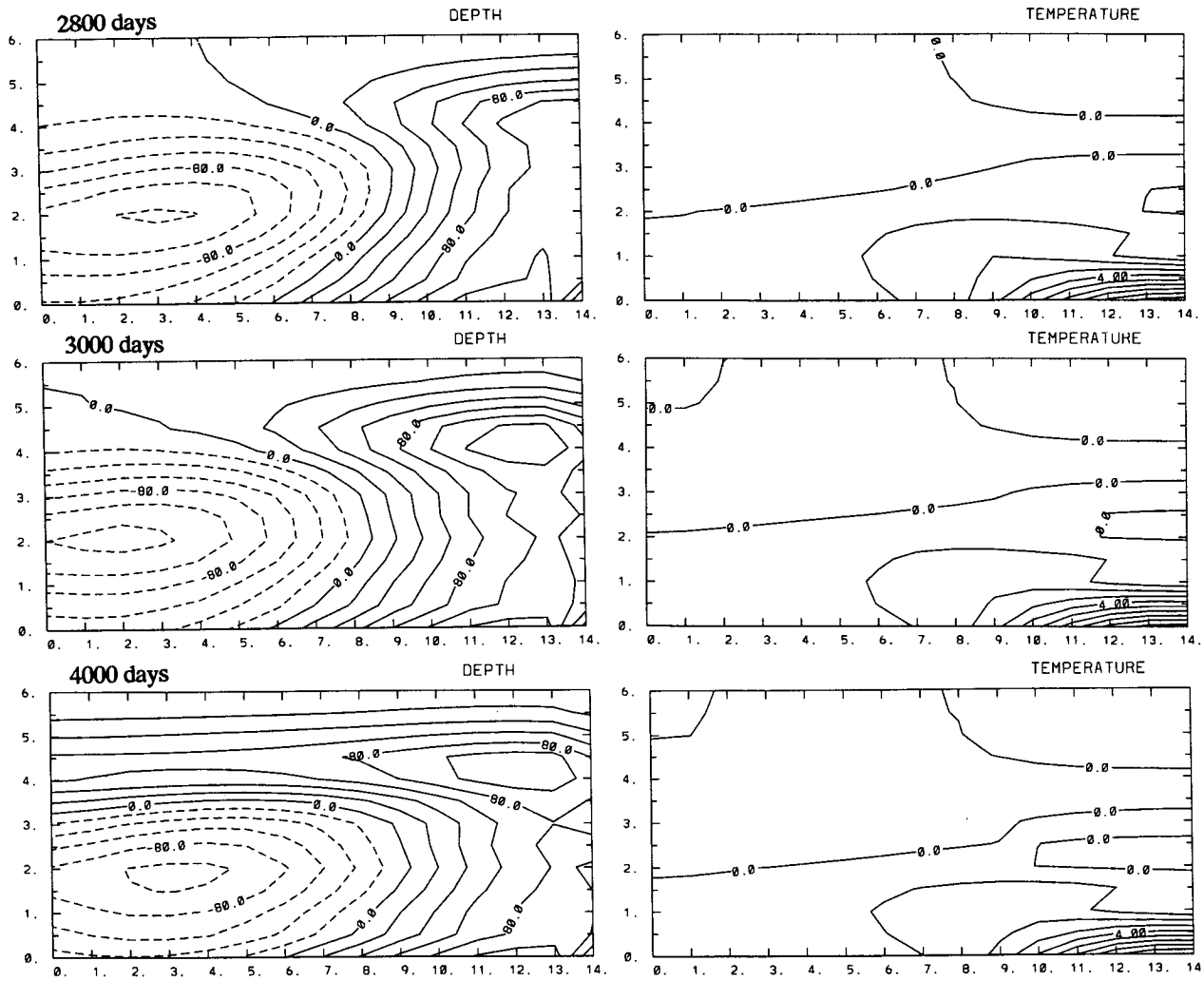

FIG. 7. (*Continued*)

be extended to consider the asymmetry between the warm and cold states. In future work this extended delayed oscillator equation and its applicability to the results described in this paper will be presented.

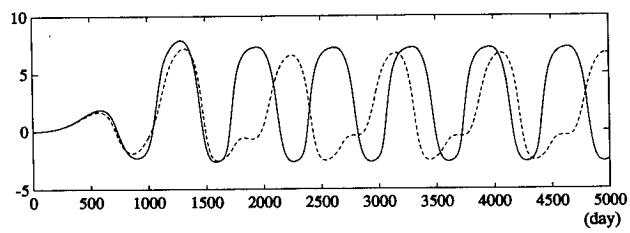

FIG. 8. The dotted line shows the time series of SSTA in the eastern basin for the case in which the coupling is weakened according to Eq. (8). The solid line is the control run for the standard case. In both $K_Q = 1600$ and $\delta = 1$ (point C in Fig. 1).

Acknowledgments. The first author appreciates the work of his students, Messrs. S. Nakahara and M. Uchida, for assisting in the numerical calculations. This work was partially supported by grants from the NOAA TOGA Office and from the NOAA Equatorial Pacific Ocean Climate Studies (EPOCS) program to the University of Washington Experimental Climate Forecast Center and a grant in Aid for Scientific Research from the Ministry of Education of Japan.

REFERENCES

Anderson, D. L. T., and J. P. McCreary, 1985: Slowly propagating disturbances in a coupled ocean–atmosphere model. *J. Atmos. Sci.*, **42,** 615–629.

Battisti, D. S., and A. C. Hirst, 1989: Interannual variability in a tropical atmosphere–ocean model: Influence of the basic state, ocean geometry and nonlinearity. *J. Atmos. Sci.*, **46,** 1687–1712.

Hirst, A. C., 1988: Slow instabilities in tropical ocean basin–global atmosphere models. *J. Atmos. Sci.,* **45,** 830–852.

Suarez, M. J., and P. S. Schopf, 1988: A delayed action oscillation for ENSO. *J. Atmos. Sci.,* **45,** 3283–3287.

Wakata, Y., 1989: On the instability problem in simple atmosphere–ocean coupled models with an oceanic surface boundary layer. *J. Meteor. Soc. Japan,* **67,** 313–324.

——, and E. S. Sarachik, 1991a: On the role of equatorial ocean modes in the ENSO cycle. *J. Phys. Oceanogr.,* **21,** 434–443.

——, and ——, 1991b: Unstable coupled atmosphere–ocean basin modes in the presence of a spatially varying basic state. *J. Atmos. Sci.,* **48,** 2060–2077.

Zebiak, S. E., and M. A. Cane, 1987: A model El Niño–Southern Oscillation. *Mon. Wea. Rev.,* **115,** 2262–2278.